https://doi.org/10.53964/jmn.2023002

https://www.innovationforever.com

Journal of Modern Nanotechnology

ISSN 2788-8118 (Online)

Open Access

Research Article

Effects of Heat Treatment in Air Atmosphere on Dip Coating Deposited CdS Thin Films for Photo Sensor Applications

Madhavi Sharad Darekar[1*], B M Praveen[1]

[1]Department of Nanotechnology, Institute of Engineering and Technology, Srinivas University, Mangalore, Karnataka, India

[*]**Correspondence to: Madhavi Sharad Darekar, PhD (Physics), Post Doctoral Fellow,** Department of Nanotechnology, Institute of Engineering and Technology, Srinivas University, Mukka, Surathkal, Mangalore 574146, Karnataka, India; Email: madhavi_darekar28@rediff.com

Received: November 27, 2022 **Revised:** March 5, 2023 **Accepted:** March 20, 2023 **Published:** April 20, 2023

Abstract

Objective: In this report, photo sensitive materials with enhanced charge carriers have been prepared using dip coating technique.

Methods: Cadmium sulphide (CdS) is N-type semiconductor compound belonging to II-VI group. CdS nanoparticles were synthesized using non-aqueous chemical method and characterized by ultraviolet-visible (UV-Vis) absorption spectroscopy, photoluminescence (PL) and transmission electron microscopy. CdS films were deposited on fluorine doped tin oxide (FTO) glass slides using dip coating method at different dip times and heat treated in air and analyzed by X-ray diffraction (XRD), scanning electron microscopy (SEM), energy dispersive analysis by X-rays (EDAX), mapping and atomic force microscopy (AFM).

Results: Quantum confinement effect was observed in UV-Vis absorption spectra of CdS nanoparticles. Quenching of luminescence intensity and blue shift at smaller wavelengths were observed in PL spectra. Presence of highly dense rectangular shaped grains in CdS films and increment in particle sizes with increase in dip time were shown by AFM images. Selected area electron diffraction images showed ring patterns indicating polycrystalline nature of CdS nanoparticles. Increase in crystallite size and decrease in crystal defects by heat treatment in air and increment in grain size with increase in dip time were shown by SEM images. XRD analysis of CdS films showed polycrystalline nature.

Conclusion: In previous work, preparation of dip coating deposited CdS films on FTO glass substrates for optoelectronic device applications such as photo sensors has not been reported. In this study, I-V characteristics of heterojunctions under dark and illumination conditions were discussed. Experimental results obtained in our study and their comparison with previous reports were also discussed.

Keywords: synthesis, characterization, nanoparticles, CdS thin films, photo sensors, dip coating method

https://doi.org/10.53964/jmn.2023002

Citation: Darekar MS, Praveen BM. Effects of Heat Treatment in Air Atmosphere on Dip Coating Deposited CdS Thin Films for Photo Sensor Applications. *J Mod Nanotechnol*, 2023; 3: 2. DOI: 10.53964/jmn.2023002.

1 INTRODUCTION

Cadmium sulphide (CdS) is chalcogenide n-type semiconductor belonging to II-VI group and it has a wide direct band gap of 2.42 eV at room temperature. CdS is used in various applications such as solar cells, optical detectors[1], semiconductor lasers, display devices, biological sensing[2], nanopiezoelectrical devices[3] as window layers in photovoltaic cells, thin film field effect transistors, transparent conducting semiconductor for opto-electronic devices, optical filters, multilayer light emitting diodes, a buffer layer is widely used as an n-type hetero-junction partner in all chalcopyrite based thin film solar cell, light detectors etc[4].

Some of the interesting size dependent properties like geometrical structure, bonding, ionization energy, band gap in semiconductors or insulators, magnetic moment, melting point, mechanical properties, electronic structure etc. are observed in semiconductor nanoparticles when the size of the particles is comparable with or smaller than the Bohr diameter of exciton for that material. The Bohr radius of exciton for CdS is 2nm. The quantum size effect is observed when the size of the particles is comparable with or smaller than 4nm. Due to these properties, CdS nanoparticles were used in abundant applications than the other nanoparticles.

The literature shows that, the various techniques like molecular beam epitaxy, chemical bath deposition (CBD), pulsed direct current magnetron, sputtering, R.F. sputtering, electrochemical atomic layer deposition, metal-organic chemical vapour deposition, close-space sublimation, coating by using nanocrystal ink, close spaced vapour transport, successive ionic layer adsorption and reaction method, dip coating method, modified chemical bath deposition (MCBD), chemical vapour deposition, photochemical deposition, thermal evaporation, radio frequency sputtering, ultrasonic spray pyrolysis, sol-gel spin coating, pulsed-laser deposition, solvethermal method, spray pyrolysis, screen printing, physical vapour deposition, spin coating method, electro deposition, laser ablation, sputtering, vacuum evaporation, MCBD, vacuum deposition, metal-organic chemical vapour deposition, electrochemical atomic layer epitaxy etc.[1,3-8] have been used to prepare CdS thin films. The advantages of dip coating method for the deposition of thin films as compared to the other methods are its simplicity, low cost instrumentation, deposition of large area thin films, use of same solution, availability of starting materials etc[9,10].

In the present study, the non-aqueous chemical method was used to synthesize CdS nanoparticles having different sizes and energy gaps by changing the molarity of thioglycerol acting as the organic capping agent at room temperature. These nanoparticles were analysed by ultraviolet-visible (UV-Vis) absorption spectroscopy, photoluminescence (PL) and transmission electron microscopy (TEM). The dip coating method was used to deposit CdS thin films on polycrystalline fluorine doped tin oxide (FTO) glass slides at different dip times and these thin films were heat treated in air atmosphere and investigated by X-ray diffraction (XRD), scanning electron microscopy (SEM), energy dispersive analysis by X-rays (EDAX), mapping and atomic force microscopy (AFM). The dip coating method was used for film deposition because of its simplicity, cost favourable instrumentation, utility of same solution and large area thin film deposition[9].

Due to unique chemical and physical properties, the nanocrystalline materials were fabricated with considerable interest in the field of materials research over the past decade[11]. The properties of nanoparticles can be used in many applications in the fields of science, engineering, medicine and environment. The major properties of nanoparticles are: (1) optical properties, (2) electrical properties, (3) magnetic properties, (4) structural properties, and (5) mechanical properties etc. Interesting and technologically useful new devices like non-volatile or single electron transistor have been developed due to size dependent properties. This helps to understand the formation of solid from an atom, molecules, group of molecules or clusters and also it helps to understand the changes in the structure, bonding, electronic structure and other properties during the evolution. Today, the semiconductor devices are used in a large range of applications like kitchen appliances, medical applications, worships, space crafts etc.[12].

Shahzad et al.[13] studied the flow nature of blood based hybrid nano fluid which consists of two or more nanoparticles through a stenosed artery having permeable walls. The entropy generation is studied to observe the disorder of system The flow behaviour of hybrid nano fluid was examined mathematically. The major findings of this work are: (1) To increase the height of stenosis, the fluid moves quickly through the artery. (2) To get the higher values of slip parameter, Darcy number and electro-osmotic parameter near the axis, the fluid moves slowly through the artery. The behaviour of the fluid flow reverses near the walls. (3) The behaviour of the flow velocity is axisymmetric. (4) Temperature becomes high near the axis of channel and it becomes zero on

the boundary. (5) For the symmetric shape of stenosis, the value of temperature increases rapidly as compared to the non-symmetric shape. (6) The lowest disorder was shown near the mean of channel by the entropy analysis. The disorder increases on the radial axis and it becomes higher on the walls[13]. The electro-osmotically modulated hemodynamic inside a stenosed artery was explained by Saleem et al. by considering both cases of symmetric and nonsymmetric shapes of stenosis[14]. The mathematical investigation of the peristaltic flow of carbon nanotubes in an elliptic duct with ciliated walls was interpreted by the Cartesian coordinate system approach. It was observed in all velocity graphs that an axially symmetry flow is a fully developed flow and the velocity becomes zero near the walls of duct. The thermal conductivity of base fluid increases and the temperature of the fluid decreases with an increase in carbon nanotubes in the base fluid. An axial symmetry profile of temperature was observed in all temperature graphs. There is a maximum increment in temperature in the centre of duct and a decrement in temperature to zero at the duct walls[15]. The mathematical interpretation of the flow of a heated Newtonian viscous fluid with single wall carbon nanotubes inside a vertical elliptical duct with sinusoidally deformable walls shows the increment in the thermal conductivity with the use of carbon nanotubes in the base fluid. The results of this study are: The behaviour of an axially symmetric flow which is the peristaltic flow in the vertical elliptic duct was seen in the temperature graphs. There is an enhancement in the volume fraction of carbon nanotubes in the base fluid and a decrement in the temperature of fluid due to the high value of thermal conductivity of carbon nanotubes[16].

A photo sensor is a type of electronic component that enables the detection of light, Infrared (IR) and other forms of electromagnetic energy. The light sensor is a passive device that converts the light energy into an electrical signal output. Light sensors are more commonly known as Photoelectric Devices or Photo Sensors because they convert light energy (photons) into electronic signal (electrons). Phototransistors, photoresistors, and photodiodes are some of the more common type of light intensity sensors.

Photoelectric sensors use a beam of light to detect the presence or absence of an object. It emits a light beam (visible or IR) from its light-emitting element. A reflective-type photo electric sensor is used to detect the light beam reflected from the target. A beam of light is emitted from the light emitting element and is received by the light receiving element. Both the light emitting and light receiving elements are contained in a single housing. The sensor receives the light reflected from the target.

The working principle of a photoelectric sensor is to change the intensity of light into electrical signals by using a photoelectric component like a conversion element. This sensor is composed of three main parts transmitter, receiver and detection circuit. The transmitter in this sensor emits a light ray to the object and the emitted light ray is usually a semiconductor light source like an LED, a laser diode and an IR diode. The ray is emitted constantly otherwise changes the pulse width to achieve it. The receiver commonly includes a photodiode, a photocell, and a phototransistor. Ahead of the receiver, optical components are installed like lens and aperture. At the back of the receiver, a detection circuit is used where this circuit filter outs the effective signal and make appropriate actions.

A photoelectric sensor consists primarily of an emitter for emitting light and a receiver for receiving light. When emitted light is interrupted or reflected by the sensing object, it changes the amount of light that arrives at the receiver. The receiver detects this change and converts it to an electrical output.

A photoelectric sensor is a device used to determine different objects, the absence, or presence of an object, changes within surface conditions and measure the distance between an object and a point and other devices with different optical properties by using a light transmitter, often IR, and a photoelectric receiver. So, these sensors are largely used in industrial manufacturing because they provide reliable and quick results without touching the object physically. A photoelectric sensor is a device that detects a difference in the light level received from the light source. The sensor is made up of a light source, an amplifier, signal converter, and an output.

A phototransistor, on the other hand, uses the level of light it detects to determine how much current can pass through the circuit. So, if the sensor is in a dark room, it only lets a small amount of current to flow. If it detects a bright light, it lets a larger amount of current flow. A photoresistor is made of CdS whose resistance is maximum when the sensor is dark. When the photoresistor is exposed to light, its resistance drops in proportion to the intensity of light. When interfaced with a circuit and balanced with potentiometer, the change in light intensity will show up as change in voltage. These sensors are simple, reliable, and cheap, used widely for measuring light intensity.

A photo electric sensor is used in electronic and computing devices to receive input and / or transmit data in the form of light or electromagnetic signals. Photo sensors are also known as photo detectors. Typically, photo sensors help in detecting change or intensity of electromagnetic energy or signals transmitted from

a sending device. Depending on the receiving or interpreting device, this change or intensity of light results in a specific action. For example, when an infrared-based remote control transmits a signal to the television, the photo sensor in the TV translates it into an action such as increasing or decreasing volume or changing channels. Some of the common electronic and computing devices and technologies that utilize photo sensors are: (1) optical disk drives, (2) fiber optics, (3) remote control devices, and (4) wireless networks.

Photoelectric sensors can be used in many different ways and industries. For example, they can be used to detect objects or the orientation of an object on a production line, they can be used to count, and they can also be used to stop automatic closing doors and elevators. For instance, buses have automatic doors that detect the motion of passerby and open and close automatically. This is made possible with the help of photoelectric sensors; they scan the entire area around the doorway and open and close when they detect motion (i.e., when people board or deboard the bus). Photoelectric sensors are used in the automotive, food, transportation, and material handling industries. They can be used to detect most materials like metal, plastic, and wood. They can even detect clear items like glass, plastic, and liquids depending on what type of sensor it is.

Sensitivity, velocity, and spectral response are the three primary characteristics of photoelectric sensors. (1) Sensitivity: The sensitivity of photoelectric sensors is associated with the magnitude of the output, which varies with the intensity of light hitting the sensor. The sensitivity is the ratio of the magnitude output to the input magnitude. (2) Velocity: Photoelectric sensors are designed to detect the rapid variations of light, and their response speed/velocity is an essential factor in certain applications. (3) Spectral response: The third primary characteristic of a photoelectric sensor refers to its ability to "see". A good majority of photoelectric sensors in the market today can detect both IR and ultraviolet radiation.

The advantages of photoelectric sensor are: (1) It senses all kinds of materials; (2) It has a longer life; (3) It has a long sensing range and is very reliable; (4) It has a very fast response time; (5) It is less costly; and (6) Diffuse photoelectric sensor detects small objects including color mark and label detection.

In this study, we have discussed about the preparation of photo sensitive materials with enhanced charge carriers by using the dip coating method.

2 MATERIALS AND METHODS

The dimensions of the nanoparticles can be reduced in one direction to obtain thin films, in two directions to obtain wires or in all the three directions to obtain dots. Confinement of electrons to small dimensions leads to quantization of energy. In the case of three dimensional periodic bulk materials the electrons can move in all three directions i.e. there is no confinement of electrons. The role of capping agent in isolating the nanoparticles is extremely important. If a capping molecule binds in some way to a growing particle it may stick there, arrest the growth and isolate it from the other growing particles in the reaction. Thus an ideal capping molecule should reside on the surface of a particle. It forms a strong enough bond with the particle surface so that it remains there permanently, but it should not take part in any other process occurring inside the particle. In other words, it should just be able to avoid the coalescence of nanoparticles. The colloidal solutions of nanoparticles used in chemical methods are filtered or centrifuged and dried. Nanoparticles of different sizes can be obtained by varying the molarity of the capping agent and keeping the molarities of the starting materials. The change in the molarity of the capping agent has an interesting effect on the originally colored materials. Nanoparticles can be more appropriately defined as an aggregate of atoms between 1nm and 100nm. When the particle size is comparable with or smaller than the Bohr diameter of exciton for that material, the particles show different properties. In bulk material, electron and hole easily become free at room temperature by thermal energy. In this material, the surface to bulk atom ratio is very low, but in nanosized particles, the excitonic level lies below the conduction band minimum and surface to bulk atom ratio is very high. So it is possible to utilize the unusual properties of surface atoms to enhance certain reactions in catalysis. The terminology which is used for very small clusters i.e., Highest Occupied Molecular Orbital and Lowest Unoccupied Molecular Orbitals instead of top of valence band and bottom of conduction band in case of extended solid. It should also be mentioned that in nanoparticles the energy levels are discrete levels rather than broad bands as in bulk solids. The optical absorption spectra of semiconductor nanoparticles are usually sharper as compared with bulk semiconductors[12].

Among various nanoparticles great interest has been shown towards CdS nanoparticles because of availability of discrete energy levels, size dependent optical properties, tunable bandgap and well-developed synthetic protocol, easy preparation technique with good chemical stability. CdS nanoparticle shows size dependent optical and electrical properties due to its high surface area to volume ratio and quantum confinement. Due to its very high photosensitivity it has usage in detection of visible radiations, in light emitting diodes, solar cells, photochemical catalysis[17], gas sensors,

various luminescence devices, optoelectronic devices and range of biological applications[9]. CdS is an important semiconductor photocatalyzer. Among the nanocrystalline semiconductors, CdS is investigated because of its importance in the field of nonlinear optics, thin-film transistors[6], gas detectors, optoelectronics and as window material for hetero-junction solar cells due to its high absorption coefficient.

2.1 Synthesis Using the Non-aqueous Chemical Method

Figure 1 shows the flowchart for the synthesis of thioglycerol capped CdS nanoparticles (sample a). The non-aqueous solutions of cadmium acetate (0.1M), thioglycerol (2.856M) and sodium sulphide (0.1M) were stirred in the reaction vessel by using a magnetic stirrer at room temperature under nitrogen atmosphere to avoid the oxidation of nanoparticles. While weighing the Analytical Reagent (A.R.) grade chemicals, an accuracy of 10^{-5}gm was maintained and in volumetric measurements accuracy was up to 10^{-1}mL. The centrifuge machine was used to separate the supernatant and the precipitate. All 1-thioglycerol stabilized CdS particles were washed three times with acetone and three times with diethyl ether and transformed to petri dish and vacuum dried. CdS nanoparticles were obtained in powder form. CdS nanoparticles (samples a, b and c) with different sizes and energy gaps were obtained by changing the concentration of thioglycerol. In sample b, the thioglycerol concentration is 1.904M and in sample c it is 0.952M. The ratio of molarities of cadmium acetate to sodium sulphide was kept constant[18].

2.2 Preparation of CdS Thin Films

A thin film of CdS nanoparticles (sample a) approximately 100nm in thickness was deposited on the pre-cleaned FTO glass substrate with 1000 dip times by using the dip coating method. Similarly CdS films approximately 200nm in thickness (sample b) and 300nm in thickness (sample c) were deposited on FTO glass substrates with 2000 dip times and 3000 dip times respectively and considered as the promising candidates for photo sensor application. Then the substrates were dried by using IR lamp and heat treated in air atmosphere at 420°C for 20 minutes. Before heat treatment in air atmosphere CdS nanoparticles are randomly arranged on the surface of FTO glass substrate and after heat treatment in air atmosphere at 420°C those nanoparticles are arranged in an ordered array. The size of the CdS nanocrystallites increases due to the coagulation phenomenon. Heat treatment in air atmosphere increases the crystallinity of CdS thin films and decreases the band gaps, resistivities and crystal defects of films[18]. Similar observations have been made by Shaikh et al.[3]. An increase in dip time increases the film thickness and the grain size and decreases the optical energy gap. Thin film thicknesses were experimentally measured by using laser profilometer[18].

Cadmium acetate dihydrate and thiourea were dissolved in methanol to prepare the precursor solution. The dip coating method was used to deposit the CdS thin films on the pre-cleaned glass substrates by using that precursor solution[4]. A.R. grade chemicals like cadmium acetate as a source of Cd and thiourea as a source of S were dissolved in methanol to prepare the precursor solution. The dip coating method was used to deposit the CdS thin films on the organically cleaned glass substrates by using that precursor solution[6] due to its simplicity, low cost and availability of starting materials[10]. The precursor solution was prepared by dissolving the A.R. grade chemicals like cadmium acetate dihydrate, thiourea, triethanolamine and ammonia and the dip coating method was used to deposit CdS thin films on the pre-cleaned glass slides by using that precursor solution due to its simplicity, low cost instrumentation, large area deposition and same solution use[3]. The CdS samples were dissolved in distilled water to prepare the precursor solutions and the expensive spin coating method was used to deposit CdS thin films on the glass substrates by using those precursor solutions[19]. In the present study, the CdS nanoparticle powders were dispersed in ethanol to prepare the precursor solutions and the dip coating method was used to deposit the CdS thin films on the pre-cleaned FTO coated glass slides by using those precursor solutions by maintaining the accuracy.

3 RESULTS AND DISCUSSION

3.1 Ultraviolet-Visible Absorption Spectroscopy

The variation of optical absorbance against the wavelength is shown in Figure 2. The UV-Vis absorption spectra of CdS nanoparticles i.e. samples a, b and c [Figure 2(a-c)] indicate that the absorption is high in the ultraviolet region of the spectra and it is very low near IR domain. This is a good property due to which the CdS film can be used as window layer in optoelectronic devices like solar cells[8]. The spectral range used in this characterization was 200 to 600nm. The CdS samples used in this case were in the form of solutions prepared by dispersing the CdS nanoparticle powders in double distilled water used as the reference solution[18]. The thioglycerol concentrations in samples a, b and c are 2.856M, 1.904M and 0.952M respectively.

The energy gap of the nanoparticles was found out by the equation of energy of a photon, $E=h\nu$ (Planck's quantum theory of radiation)[19]. An intense UV-Vis absorption peak was observed at 290nm (energy gap eV) in sample a. The UV absorption peak was observed at 310nm (energy gap ~ 4.00 eV) in sample b and the UV absorption peak was observed at 380nm (energy gap 3.26 eV) in sample c. The energy gap variation between

https://doi.org/10.53964/jmn.2023002

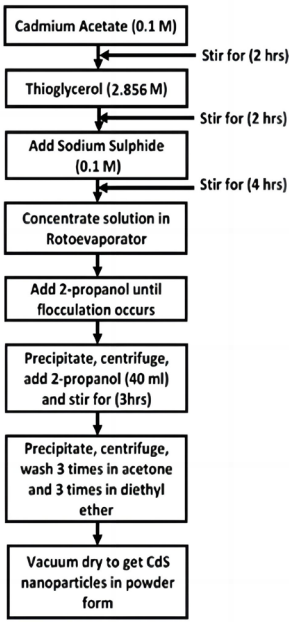

Figure 1. Procedure for the synthesis of CdS nanoparticles (sample a).

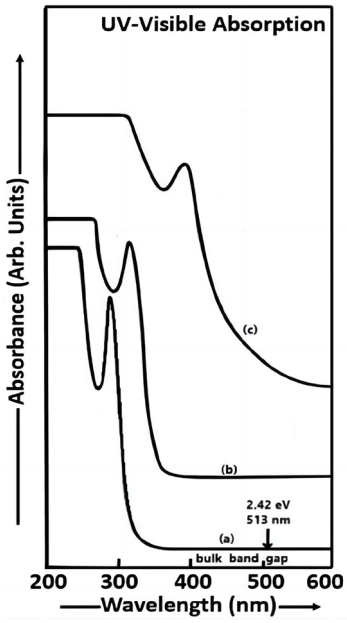

Figure 2. UV-visible absorption spectra of CdS nanoparticles (a) sample a, (b) sample b and (c) sample c.

2.42 eV to 4.28 eV was observed in CdS nanoparticles. The sizes of the CdS particles in samples a, b and c are 4.264nm, 4.464nm and 5.22nm respectively.

The band gap (E_g) of bulk CdS material is 2.42 eV at room temperature and its UV-Vis absorption peak is observed at 513nm. From Figure 2, it is clearly seen that the blue shift is observed in the optical absorption spectra of CdS nanoparticles (samples a, b and c) due to the quantum confinement in CdS nanocrystallites. There is an increase in energy gap and a decrease in particle size with an increase in thioglycerol concentration. High absorbance is observed in sample a as compared to that in samples b and c due to the higher concentration of thioglycerol. The energy gap of CdS nanoparticles prepared by Saraf[20] using the aqueous chemical method is higher than that of CdS nanoparticles synthesized in our study. The blue shift was observed at smaller wavelengths in the UV-Vis absorption spectra of CdS nanoparticles obtained in the present study as compared to the UV-Vis absorption spectra of as-deposited and annealed CdS nanocrystalline thin films at different temperatures by Shaikh et al.[3]. The blue shift was observed at higher wavelengths in the optical absorption spectra of the CBD and dip coating as-deposited CdS thin films prepared by Khimani et al.[9] in comparison with the UV-Vis absorption spectra of CdS nanoparticles obtained in our study. The difference in the values of absorption wavelengths depends on the preparation methods.

3.2 Photoluminescence

The PL spectra of CdS nanoparticles (samples a, b and c) recorded at room temperature are shown in Figure 3 (a-c).

The range of excitation wavelength and the range of emission wavelength used in sample c were 222 to 247nm and 247 to 750nm respectively. The CdS particles were excited at 232nm and the intensity of the emission peak located at 467nm (energy gap ~ 2.66 eV) starts increasing in sample c. The range of excitation wavelength and the range of emission wavelength used in sample b were 267 to 292nm and 292 to 750nm respectively. The CdS particles were excited at 277nm and the intensity of the luminescence peak observed at 466nm (energy g ~ 2.665 eV) increases by the addition of thioglycerol. The range of excitation wavelength and the range of emission wavelength used in sample a were 318 to 343nm and 343 to 750nm respectively. The CdS particles were excited at 328nm and there was a decrease in the intensity of the emission peak observed at 467nm (energy gap ~ 2.66 eV) for the small sized particles (sample a). Thus the quenching of the luminescence intensity is observed in samples c, b and a. In samples c and b, the PL intensity is increased which is attributed to sulphur ion vacancies. The emission peaks at around ~ 2.66 eV in samples c and b may be due to deep level emission which is attributed to the crystalline defects arising due to sulphur vacancies. The sulphur vacancy creates because of sulphur deficiency which leads to radiative transition in the visible region. This radiative transition matches with the emission peak wavelength observed (at around ~ 2.66 eV) in samples c and b[9]. In sample a, the PL intensity is decreased due to the removal of sulphur ion vacancies by thioglycerol. In bulk CdS material, the UV-Vis absorption peak appears

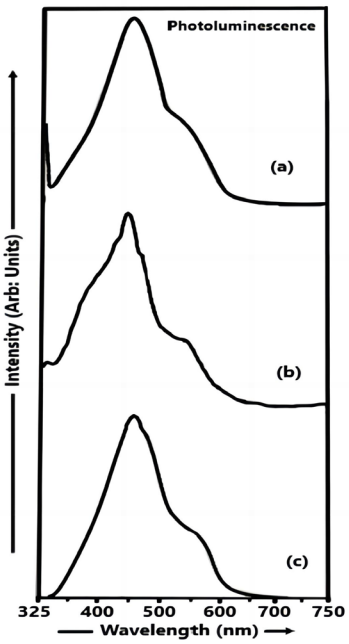

Figure 3. Photoluminescence spectra of CdS nanoparticles (a) sample a, (b) sample b and (c) sample c.

at 513nm (E_g=2.42 eV) at room temperature. Thus the blue shift is observed in Figure 3. The blue shift was observed at smaller wavelengths in the PL spectra of CdS nanoparticles obtained in our study as compared to the PL spectra of CBD and dip coating deposited CdS films prepared by Khimani et al.[9]. The blue shift was also observed at smaller wavelength in the PL spectra of CdS nanoparticles obtained in the present study in comparison with the PL spectrum of CdS nanoparticles synthesized by using the aqueous chemical method by Gurnani et al[21].

3.3 Atomic Force Spectroscopy

2D-AFM images (A) and 3D-AFM images (B) of CdS films (samples a, b and c) are shown in Figure 4(a-c). 2D-AFM images show the presence of highly dense rectangular shaped grains in the prepared CdS films. Hills and valleys are present in CdS films which are shown by 3D-AFM images. AFM images of CdS films show an increment in the particle sizes with an increase in dip time[18]. The range of the average size of the material grains which are present in CdS films is 31-210nm with different magnifications. The size of material grains of CdS film shown in [Figure 4 (a) 3D-AFM images (B) of sample a] is 36.55nm, that of CdS film shown in [Figure 4 (b) 3D-AFM images (B) of sample b] is 46nm and that of CdS film shown in [Figure 4 (c) 3D-AFM images (B) of sample c] is 90.91nm.

The 2D and 3D-AFM images of CdS thin films showed the discontinuity in dip coating deposition which limits the grain size and height [Figure 4A and B, samples a, b and c]. Similar observations were found in the AFM images of dip coating deposited CdS thin films prepared by Khimani et al. They also observed the large sized grains and large hill heights with continuity in thin film deposition shown by 2D and 3D-AFM images of CdS thin films prepared by CBD on the glass slides. The average roughness and the root mean square roughness were provided by the AFM analysis. The roughness of the CdS film surface is increased due to the growth of the initial nucleation after each dip in case of dip coating deposited CdS films[9].

3.4 Transmission Electron Microscopy

Figure 5 shows the TEM images (A) and the Selected area electron diffraction(SAED) patterns (B) of CdS nanoparticles (samples a, b and c). These smaller grains become large grains of the size up to 163nm having spherical shape in CdS layers after heat treatment in air atmosphere. The spherical shaped CdS particles of different sizes were observed at magnification of 200nm. From Figure 5A, it is clearly seen that the particle size increases with an increase in dip time and film thickness. The SAED images of CdS nanoparticles (samples a, b and c) show the polycrystalline nature of all three CdS samples and the dominant diffraction patterns in the TEM micrographs are indexed as (111) and (220) planes of cubic sphalerite-type CdS nanoparticles [Figure 5B]. The uniformity of films without defects or cracks are shown in the TEM images of CBD and dip coating deposited CdS thin films observed by Khimani et al. The polycrystalline nature of the CdS films indicated by the ring patterns are shown in the SAED images of those films. These rings are indexed and the planes shown by the XRD spectra of CdS films are in agreement with the indexed planes (100), (002), (101), (110) and (112)[9].

3.5 Scanning Electron Microscopy

The SEM images of CdS films (samples a, b and c) having various molarities of thioglycerol are shown in Figure 6(a-c). The scanning electron microscope was used to study the surface morphology of CdS thin films. The nano dots acquire energy to produce vibrations after heat treatment in air atmosphere. Due to these vibrations, the quantum dots collide with each other and due to these collisions, the surface energy of nano dots increases. The increased surface energy causes melting of grain boundaries and fusion of nanocrystallites form larger grains as a result of coagulation phenomenon. The small particles are rearranged and oriented periodically with a decrease in defect densities by the annealing effect[3]. The coalescence process increases the radius of the crystallites which is clearly shown in SEM images of annealed CdS films (Figure 3). Thus from Figure 6, it is observed that the crystallite size increases and the crystal defects decrease by heat treatment in air atmosphere. Shaikh et al. have reported similar findings[3]. The cylindrical grains are observed in samples a, b and c of different particle sizes due to various molarities

https://doi.org/10.53964/jmn.2023002

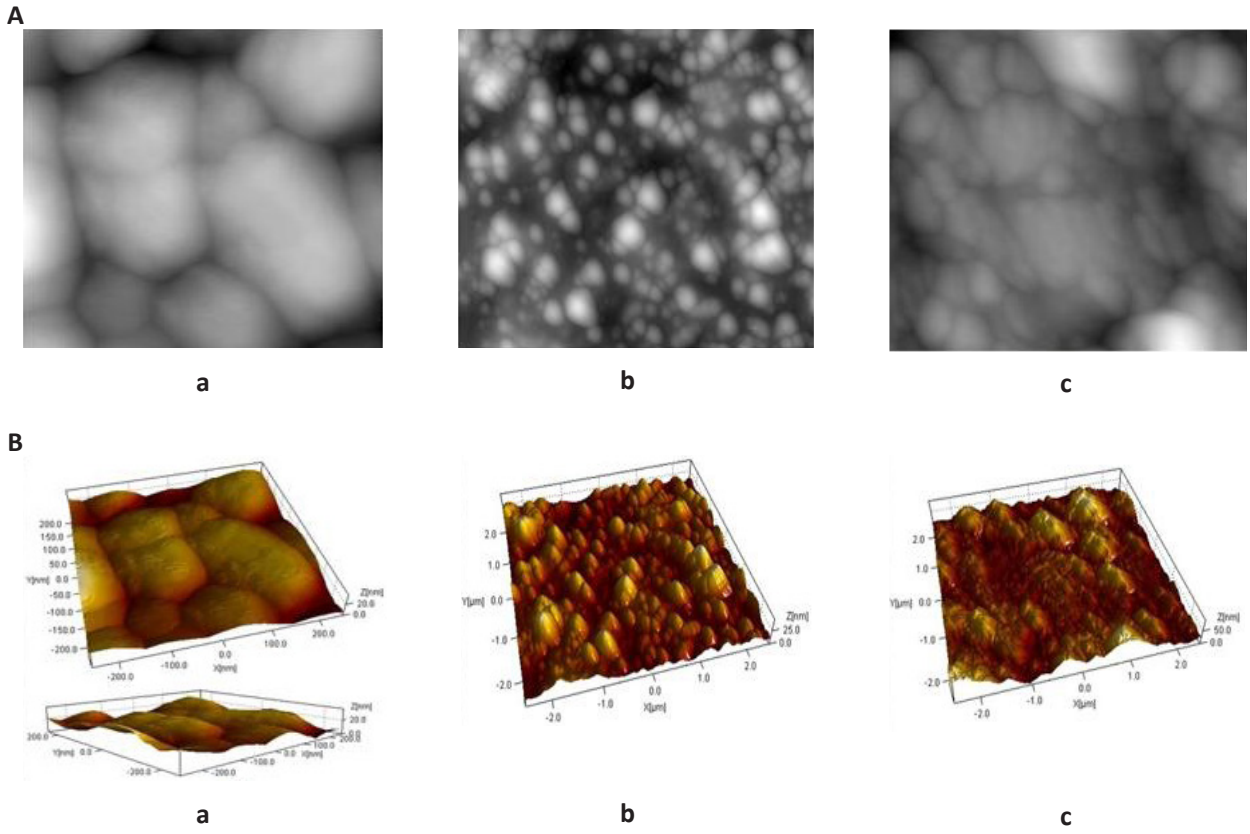

Figure 4. 2D-AFM images (A) and 3D-AFM images (B) of CdS films (a) sample a, (b) sample b and (c) sample c; with magnification of 5μm in all samples.

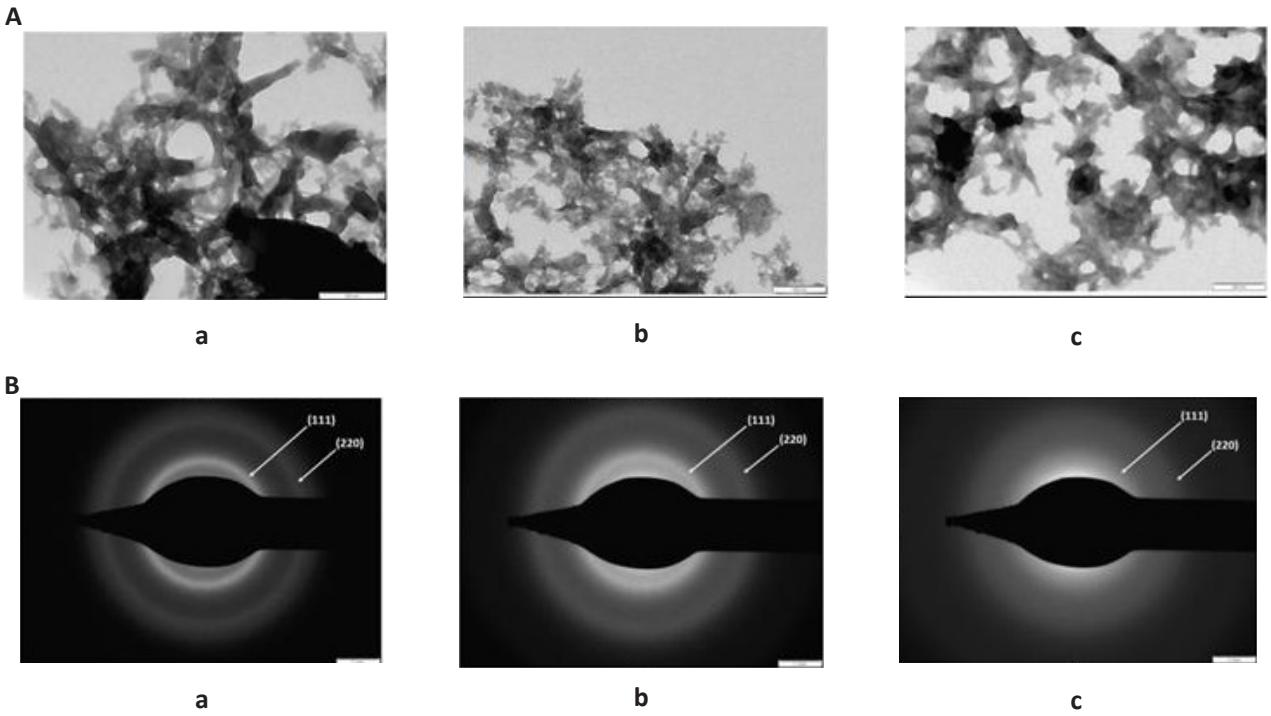

Figure 5. TEM images (A) with magnification of 200nm and SAED patterns (B) of CdS nanoparticles (a) sample a, (b) sample b and (c) sample c.

of thioglycerol. The large cylindrical grains of the size in the 24-163nm range are produced in CdS films consisting of polycrystalline CdS nanoparticles after heat treatment in air atmosphere. The large sized grains are obtained in the CdS films prepared at the highest dip time as shown in SEM images (Figure 6).

https://doi.org/10.53964/jmn.2023002

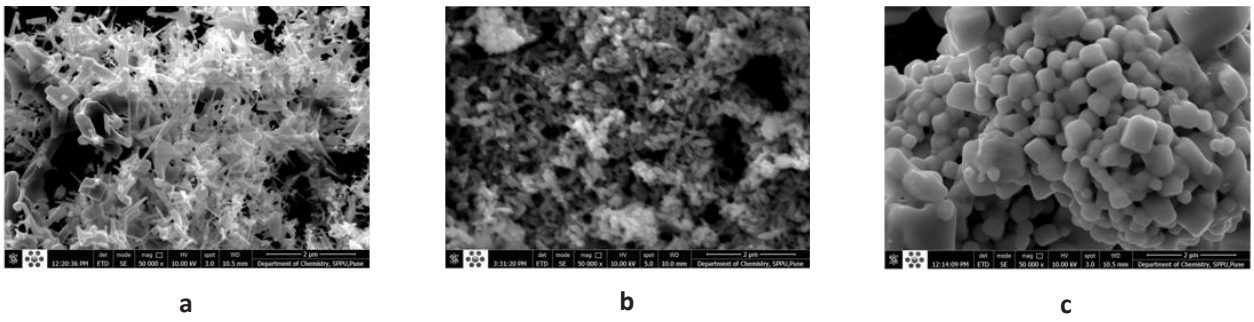

Figure 6. SEM images of CdS films (a) sample a, (b) sample b and (c) sample c; with magnification of 50,000 in all samples. Scale bar: 2μm.

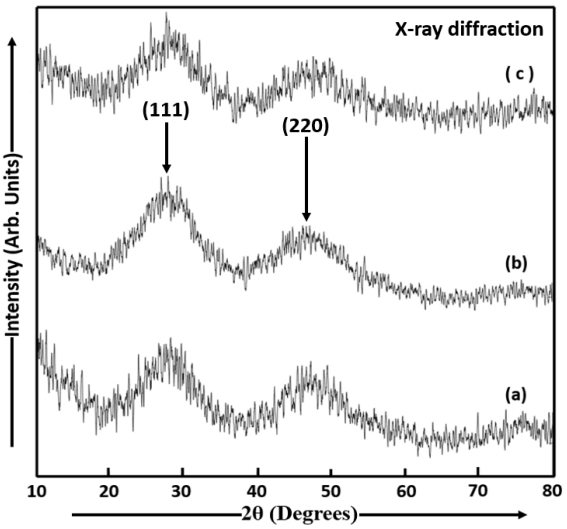

Figure 7. X-ray diffraction patterns of CdS films (a) sample a, (b) sample b and (c) sample c.

The defect densities were reduced in the CdS thin films prepared by MCBD on the glass substrates by Shaikh et al. and associates due to annealing effect[3]. Similar observations have been made in our study.

3.6 X-ray Diffraction

The XRD pattern was used to determine the crystallite size and crystal structure of the CdS nanocrystalline thin films. Figure 7 shows the XRD patterns of CdS thin films (samples a, b and c) deposited by the dip coating method. The XRD patterns of CdS films were recorded using the spectral range 5° to 80°. The polycrystalline nature of the CdS films was shown by the XRD analysis. The analysis of the powder XRD by Debye function analysis[22] shows that all the diffraction peaks were indexed to be that of CdS phase. The XRD patterns of CdS thin films (samples a, b and c) showed the preferential orientation to be along (111) direction. All three dip coating deposited CdS thin films showed the cubic sphalerite structure. The crystal structure depends on the deposition conditions[1]. The crystal structure is affected by many variables like the nature of the complex, the substrate and stirring. The degree of crystallinity was improved by the heat treatment in air atmosphere upon the CdS thin films. The smaller number of nucleation centres start to grow with a decrease in the density of nucleation centres, an increase in the grain size and a decrease in the energy gap by annealing CdS thin films[23]. The XRD peaks of CdS films were in agreement with the reported data of standard Joint Committee on Powder Diffraction Standards for CdS. The CdS particles in samples a, b and c have approximately the same average size. The crystallite sizes in CdS thin films were estimated using XRD data by the Debye-Scherrer formula, $d_{XRD} = \frac{0.9\,\lambda}{\beta \cos\theta}$ where d_{XRD} is the crystallite size, β is angular line width at half maximum intensity of the XRD peak, λ=1.542 Å is the wavelength of X-rays and θ is Bragg's diffraction angle. The determined average crystallite sizes of dip coating deposited CdS films are found to be 4.115nm in sample a, 4.098nm in sample b is and 4.097nm in sample c. The diffraction peaks are observed to be broad at half maximum intensities of the peaks. The XRD peaks having large widths indicate that the CdS films are nanocrystalline in nature. The broadening of XRD peaks is mainly due to smaller crystallite size and the lattice micro strain (ε) which depend on each other[10]. The diffraction peaks in the XRD pattern of sample a were observed at 2 θ=29.720° and 2 θ=46.060° corresponding to the {111} (d=3.0035 Å) and {220} (d=1.9690 Å) reflections of the CdS possessing cubic sphalerite structure. Similarly, the XRD peaks of sample b were observed at 2 θ=27.920° and 2 θ=46.660° corresponding to the {111} (d=3.1929 Å) and {220} (d=1.9450 Å) reflections of CdS and the XRD peaks of sample c were observed at 2 θ=27.820° and 2 θ=47.580° corresponding to the {111} (d=3.2042 Å) and {220} (d=1.9095 Å) reflections of CdS. The values of micro strain (ε) and the number of dislocation per square centimetre (δ) of CdS thin films were evaluated by using the two formulae, $\varepsilon = \frac{\beta \cos\theta}{4}$ and $\delta = \frac{1}{d_{XRD}^2}$[24]. The value of ε of sample a is 8.430×10^{-3}m, that of sample b is 8.464×10^{-3}m and that of sample c is 8.466×10^{-3}m. The value of δ of sample a is 5.905×10^{16} lines/m^2, that of sample b is 5.954×10^{16} lines/m^2 and that of sample c is 5.957×10^{16} lines/m^2.

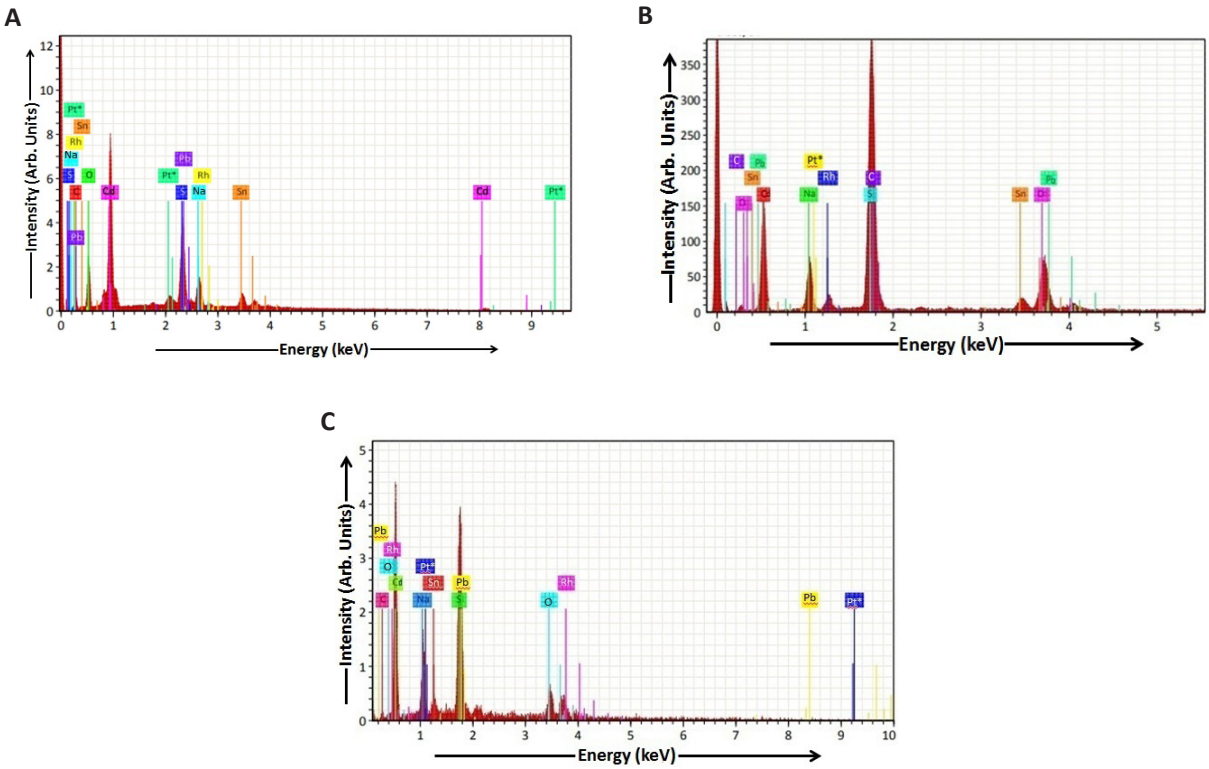

Figure 8. EDAX Spectrum of CdS film. A: EDAX Spectrum of CdS film (sample a); B: EDAX Spectrum of CdS film (sample b); C: EDAX Spectrum of CdS film (sample c).

A polycrystalline and a mixed phase of both cubic and hexagonal structure was observed in as-deposited CdS films deposited by CBD method onto glass substrates by Uplane and Pawar[25]. The average crystallite size D of dip coating deposited CdS thin films prepared in our study is smaller than that (67nm) of CdS thin films prepared by Saraf, R, using the spin coating method[20]. The average particle sizes of CdS thin films deposited on FTO glass slides by using the dip coating method in the present study are smaller than the average crystallite sizes of CBD (21.47nm) and dip coating (24.97nm) deposited CdS thin films prepared by Khimani et al.[9].

3.7 Energy Dispersive Analysis by X-rays

The EDAX spectra observed for the CdS thin films (samples a, b and c) deposited by the dip coating method are shown in Figure 8. The estimation of atomic composition of these samples was done by careful analysis of the area under each peak[26]. The spectrum of sample a showed the presence of the elements like cadmium (Cd), sulphur (S), sodium (Na), oxygen (O), carbon (C), rhodium (Rh), lead (Pb), platinum (Pt) and tin (Sn) in atomic percentage in Table 1. The spectrum of sample b showed the presence of the elements like Cd, S, Na, Rh, O, Pt, Sn, Pb and C in atomic percentage in Table 2. The spectrum of sample c showed the presence of the elements like Cd, S, C, Na, Sn, Pt, O, Rh and Pb in atomic percentage in Table 3. The Cd:S ratios for dip coating deposited CdS thin films (samples a, b and c) can be calculated from Tables 1- 3 respectively. The values of Cd:S ratios for samples a, b and c are 1.03, 1.04 and 1.05 respectively. From these values, it is clearly seen that the value of the Cd:S ratio increases with an increase in dip time and a decrease in thioglycerol concentration. It can be clearly seen that the samples a, b and c are rich in Cd relative to S. The stoichiometry of CdS thin films is nearly perfect. The values of Cd:S ratios for dip coating deposited CdS thin films prepared in our study are smaller than those values of CBD and dip coating deposited CdS thin films calculated by Khimani et al. The elements like Cd, S, Si and Ca are present in the CBD and dip coating deposited CdS thin films prepared by Khimani et al. and the presence of the elements is shown in the EDAX spectra of those CdS thin films[9].

3.8 Measurement of Photosensitivity

The light of various intensities i.e. 60W/cm^2, 100W/cm^2 and 200W/cm^2 were incident on the heat treated CdS nanoparticles coated FTO glass substrates (i.e., N-type semiconductor). The valence electrons in CdS thin films (samples a, b and c) and FTO thin films acquired sufficient energy from the incident light by absorbing the incident photons to overcome the forbidden energy gap. The covalent bonds were broken and those electrons went to the conduction band leaving holes in the valence band and the electron-hole pairs were produced. The number of electron-hole pairs increased with an increase in the intensity of the incident light. The number of electron-hole pairs produced in the presence of light having various intensities, was higher than that produced in the

Table 1. EDAX Data of CdS Thin Film (sample a)

Element	At. No.	Netto	Mass [%]	Mass Norm [%]	Atom [%]	Abs. error [%] (1 Sigma)	Rel. error [%] (1 Sigma)
Sodium	11	8189	5.19	5.05	6.41	0.22	4.19
Sulphur	16	19790	10.70	10.41	28.63	0.42	3.92
Oxygen	8	9449	10.23	9.95	14.03	1.47	14.36
Carbon	6	1646	3.35	3.26	12.22	0.69	20.61
Rhodium	45	4727	4.81	4.68	2.05	0.21	4.37
Cadmium	48	42781	42.85	41.67	29.55	5.14	11.99
Lead	82	13645	15.11	14.69	3.20	0.59	3.90
Platinum	78	4649	0.00	0.00	0.00	0.00	1.78
Tin	50	8629	10.60	10.31	3.91	0.40	3.81
Sum			102.84	100.00	100.00		

Table 2. EDAX Data of CdS Thin Film (sample b)

Element	At. No.	Netto	Mass [%]	Mass Norm [%]	Atom [%]	Abs. error [%] (1 Sigma)	Rel. error [%] (1 Sigma)
Cadmium	48	9228	37.84	16.42	37.50	5.39	14.23
Sodium	11	4203	12.47	5.41	7.60	0.82	6.59
Rhodium	45	1372	3.27	1.42	2.14	0.23	7.17
Sulphur	16	23772	58.46	25.36	36.01	2.46	4.21
Oxygen	8	5664	20.28	8.80	8.47	0.78	3.83
Platinum	78	942	3.89	1.69	0.00	0.32	8.14
Tin	50	2761	13.14	5.70	1.76	0.56	4.25
Lead	82	5112	28.59	12.40	2.55	1.10	3.85
Carbon	6	14419	52.53	22.79	3.97	2.27	4.31
Sum			230.48	100.00	100.00		

Table 3. EDAX Data of CdS Thin Film (sample c)

Element	At. No.	Netto	Mass [%]	Mass Norm [%]	Atom [%]	Abs. error [%] (1 Sigma)	Rel. error [%] (1 Sigma)
Carbon	6	71	1.22	1.03	1.52	0.73	59.69
Cadmium	48	3977	36.02	30.40	46.88	5.91	16.41
Sodium	11	1269	7.81	6.59	1.85	0.60	7.63
Tin	50	335	1.80	1.52	0.94	0.18	10.26
Sulphur	16	3667	18.18	15.34	44.64	0.87	4.79
Platinum	78	345	3.04	2.57	0.00	0.31	10.24
Oxygen	8	1405	21.99	18.55	3.44	1.04	4.75
Rhodium	45	597	10.85	9.15	0.23	0.66	6.11
Lead	82	2353	17.59	14.85	0.50	0.90	5.11
Sum			118.50	100.00	100.00		

dark condition. When this N-type semiconductor was used while preparing the P-N junction diode, the forward current (diffusion current) was measured in the case of forward biased P-N junction diode and the reverse current (dark current) was measured in the case of reverse biased P-N junction diode. The values of dark current under dark condition and photocurrent under illumination condition depend upon the number of charge carriers. There was an increase in photocurrent as compared to dark current in the presence of light of various intensities in case of photosensitive materials (CdS nanoparticles coated FTO glass slides). The dark current decreased and the photocurrent increased with an increase in dip time, film thickness and particle size. Figure 9 show the I-V

https://doi.org/10.53964/jmn.2023002

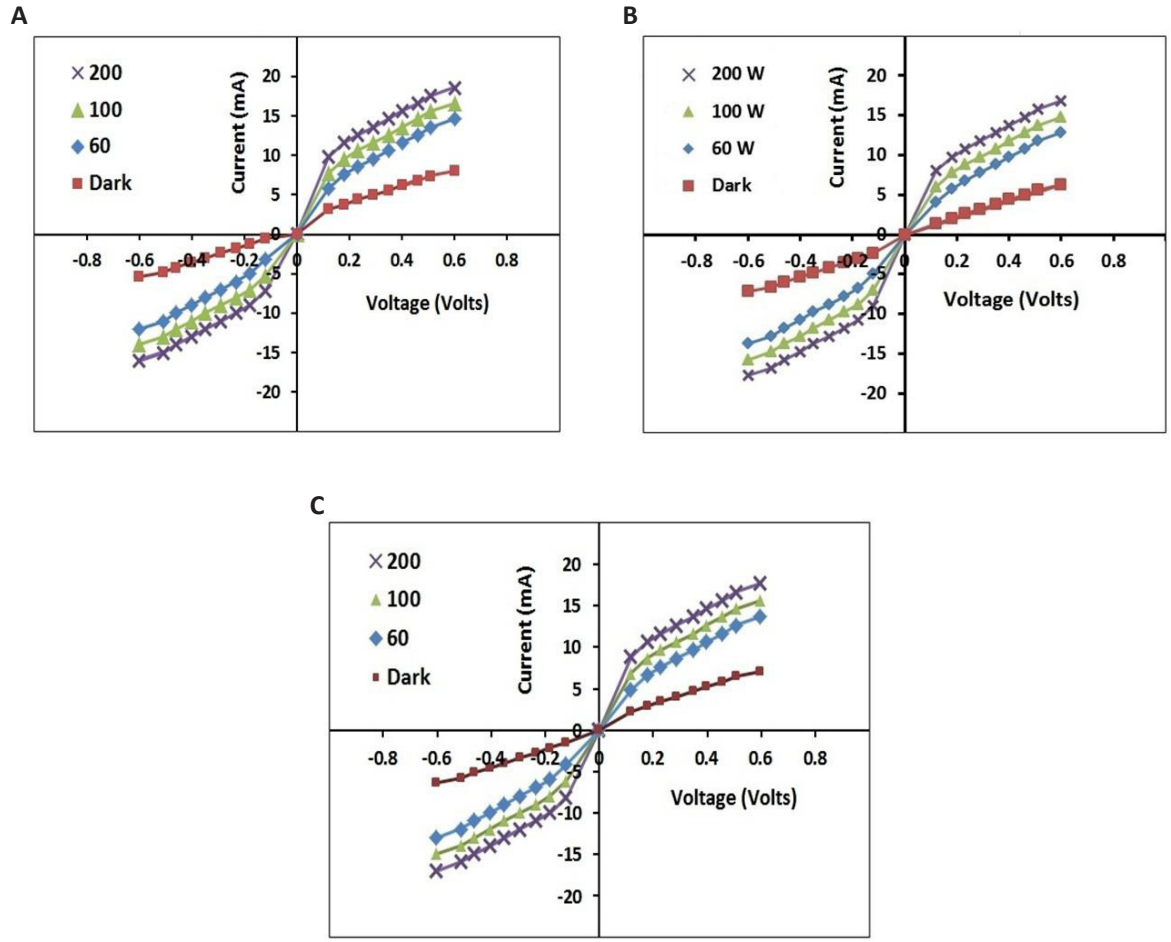

Figure 9. I-V characteristics obtained from CdS thin film. A: I-V characteristics obtained from CdS thin film (sample a) for light of various intensities; B: I-V characteristics obtained from CdS thin film (sample b) for light of various intensities; C: I-V characteristics obtained from CdS thin film (sample c) for light of various intensities.

Table 4. Photosensitivity Data of CdS Thin Film (sample a)

Resistance of Thin Film in Dark Condition (R_d) Ω	Resistance of Thin Film in the Presence of Light (R_l) Ω			Photosensitivity		
	Light Intensity (60W/cm^2)	Light Intensity (100W/cm^2)	Light Intensity (200W/cm^2)	Light Intensity (60W/cm^2)	Light Intensity (100W/cm^2)	Light Intensity (200W/cm^2)
0	0	0	0	0	0	0
102.85	25.712	13.370	10.142	0.75	0.87	0.9
105.49	36.734	24.489	20.571	0.65	0.76	0.80
110	39.285	27.329	22.448	0.64	0.75	0.79
114.28	40	30.769	25.806	0.64	0.73	0.77
117.85	42.857	31.428	27.731	0.63	0.73	0.76
121.73	43.956	35.714	30.888	0.63	0.70	0.74
125.71	44.897	36.974	31.428	0.64	0.70	0.74
128.57	45.714	38.095	31.893	0.64	0.70	0.75
171.42	46.551	38.571	33.540	0.72	0.77	0.80

characteristics obtained from CdS thin films (samples a, b and c) for light of various intensities. These I-V characteristics show the behaviour of forward biased and reverse biased P-N junction diodes.

The energy gap of CdS nanoparticles in sample a is ~ 4.28 eV, that in sample b is ~ 4.00 eV, that in sample c is ~ 3.26 eV and that of FTO film is ~ 3.8 eV. The energy gaps of CdS nanoparticles in samples a, b and c decreased after heat treatment in air atmosphere and also due to greater crystallite sizes. The energy of natural light and that of the light of various intensities were higher than the energy gaps of CdS nanoparticles in samples a, b and c and the energy gap of FTO film

Table 5. Photosensitivity Data of CdS Thin Film (sample b)

Resistance of Thin Film in Dark Condition (R_d) Ω	Resistance of Thin Film in the Presence of Light (R_l) Ω			Photosensitivity		
	Light Intensity (60W/cm^2)	Light Intensity (100W/cm^2)	Light Intensity (200W/cm^2)	Light Intensity (60W/cm^2)	Light Intensity (100W/cm^2)	Light Intensity (200W/cm^2)
0	0	0	0	0	0	0
68.181	28.571	19.047	14.285	0.58	0.72	0.79
71.146	30.252	23.376	18.367	0.57	0.67	0.74
73.089	31.428	24.175	19.642	0.55	0.66	0.73
75.067	34.782	28.571	23.529	0.53	0.62	0.68
78.571	36.263	31.015	24.812	0.53	0.60	0.68
80.808	37.833	32.323	28.282	0.53	0.60	0.65
83.809	39.285	33.523	29.235	0.53	0.60	0.65
85.714	40.336	35.142	29.813	0.52	0.59	0.65
88.524	41.698	37.180	31.486	0.52	0.58	0.64

Table 6. Photosensitivity Data of CdS Thin Film (sample c)

Resistance of Thin Film in Dark Condition (R_d) Ω	Resistance of Thin Film in the Presence of Light (R_l) Ω			Photosensitivity		
	Light Intensity (60W/cm^2)	Light Intensity (100W/cm^2)	Light Intensity (200W/cm^2)	Light Intensity (60W/cm^2)	Light Intensity (100W/cm^2)	Light Intensity (200W/cm^2)
0	0	0	0	0	0	0
42.857	17.571	14.285	11.428	0.59	0.67	0.73
51.428	22.360	17.733	15.126	0.56	0.65	0.70
52.380	24.175	19.642	16.117	0.54	0.62	0.69
57.142	27.586	22.222	19.047	0.51	0.61	0.67
58.928	29.464	24.812	20.496	0.50	0.57	0.65
63.492	32.234	27.210	23.323	0.49	0.57	0.63
64.857	32.653	27.329	24.175	0.49	0.57	0.63
66.337	33.653	27.988	24.489	0.49	0.57	0.63
67.080	34.285	29.670	26.600	0.48	0.56	0.60

so that the CdS and FTO layers were able to absorb the maximum amount of light to produce a large amount of photo-generated charge carriers. Thus, the CdS and FTO layers generated a large magnitude of photocurrent and enhanced photosensitivity. As the energy gap of sample c was lower than that of sample b and the energy gap of sample b was lower than that of sample a, the photocurrent produced in sample c was higher than that in samples b and a. The absorption wavelengths of CdS and FTO layers were in the visible region. It has been observed that there is an increase in surface roughness, thin film thickness, particle size and photocurrent and a decrease in dark current with an increase in dip time in case of photosensitive CdS thin films. The characterization results indicated an improvement in mechanical properties of CdS films.

The values of photosensitivity of heat treated CdS samples (samples a, b and c) in the presence of various light intensities were calculated by using the given formula, S = where R_d is the resistance of the thin film in dark condition and R_l is the resistance of the thin film under illumination condition. The calculated values of S and R_l for different light intensities and that of R_d of CdS thin films (samples a, b and c) are shown in Tables 4-6 respectively. From Tables 4-6, it is clearly seen that the values of photocurrent on exposure with different intensity lamps are higher than the values of current measured in dark condition and also it is observed that the photosensitivity increases with an increase in light intensity due to enhanced excitation of valence electrons and creation of electron-hole pairs. The photosensitive materials change their chemical composition and show an increase in photocurrent when exposed to electromagnetic radiation[3].

The absorption peaks were observed at approximately 500nm in the UV-Vis absorption spectra of annealed CdS thin films deposited on glass substrates using MCBD technique by Shaikh et al.[3]. The energy gap of glass substrate is approximately 9.8 eV and that of CdS films calculated by S. U. Shaikh and his associates is approximately 2.48 eV. This means that the absorption

wavelength of glass substrate (~ 126nm) is in the ultraviolet region and that of CdS film (~ 500nm) is in the visible region. So the values of photocurrent and hence photosensitivity produced in CdS thin films deposited on glass substrates using MCBD technique by Shaikh et al. are smaller than those produced in CdS thin films deposited on FTO films by the dip coating method in our study. Similarly, the values of photocurrent and photosensitivity obtained in CBD deposited CdS thin films prepared by Nikam and Gosavi[5] are lesser than those obtained in dip coating deposited CdS thin films in this study. CdS thin films prepared in our study have been found to be photosensitive which can be used in various optoelectronic applications due to their charge carrier dynamics.

4 CONCLUSION

In summary, the CdS nanoparticles and their films were analyzed using various characterization techniques. The blue shift was observed in UV-Vis absorption spectra of CdS nanoparticles having good optical properties. The quenching of the luminescence intensity and the blue shift were observed in the PL emission spectra of CdS nanoparticles. The 2D AFM images demonstrated the highly dense rectangular grains in CdS films. The 3D AFM images demonstrated the hills and valleys in CdS films. The TEM images of CdS nanoparticles demonstrated the spherical shaped particles with different sizes at high magnifications. The SAED images of CdS nanoparticles demonstrated ring patterns indicating the polycrystalline nature of the particles. The SEM images of CdS films demonstrated the cylindrical particles with different particle sizes. The XRD analysis of CdS films demonstrated that CdS nanoparticles had cubic single phase (sphalerite). The EDAX analysis of CdS thin films showed the perfect stoichiometry which remained constant with an increase in temperature and film thickness. It was observed that the photocurrent increases and the dark current decreases with an increase in dip time, film thickness and particle size in case of CdS thin films which have been found to be photosensitive materials. These CdS films can be used in various applications due to the enhancement in charge carriers.

Acknowledgements

We thank the SEM and XRD operators of Chemistry Department of Savitribai Phule Pune University for performing the SEM and XRD measurements, the Head of Chemistry Department of Savitribai Phule Pune University for providing UV Absorption and PL instruments access. Also, we thank the AFM operator of Physics Department of Savitribai Phule Pune University, the TEM operator and the operator of thin film thickness measurement of IIT Powai, Mumbai for doing the AFM, TEM and thin film thickness measurement characterizations respectively.

Conflicts of Interest

The authors declared no potential conflicts of interest with respect to the research, authorship, and / or publication of this article.

Author Contribution

Darekar MS was the main author, conceived and designed the experiments, performed the experiments, analysed and interpreted the data, contributed reagents, materials, analysis tools or data, drawn diagrams and tables, plotted graphs, wrote the paper. Praveen BM supervised the manuscript preparation process.

Abbreviation List

A.R., Analytical reagent
AFM, Atomic force microscopy
C, Carbon
CBD, Chemical bath deposition
Cd, Cadmium
CdS, Cadmium sulphide
EDAX, Energy dispersive analysis by X-rays
FTO, Fluorine doped tin oxide
IR, Infrared
JCPDS, Joint committee on powder diffraction standards
MCBD, Modified chemical bath deposition
Na, Sodium
O, Oxygen
Pb, Lead
PL, Photoluminescence
Pt, Platinum
Rh, Rhodium
S, Sulphur
SAED, Selected area electron diffraction
SEM, Scanning electron microscopy
Sn, Tin
TEM, Transmission electron microscopy
UV-Vis, Ultraviolet-Visible
XRD, X-ray diffraction

References

[1] Yücel E, Kahraman S, Güder HS. Effects of different annealing atmospheres on the properties of cadmium sulfide thin films. *Mater Res Bull*, 2015; 68: 227-233.[DOI]

[2] Mondal SP, Ray SK. Cadmium Sulfide Nanostructures for Photovoltaic devices. *Proc Natl Acad Sci Sect A Phys Sci*, 2012; 82: 21-29.[DOI]

[3] Shaikh SU, Desale DJ, Siddiqui FY et al. Effects of air annealing on CdS quantum dots thin film grown at room temperature by CBD technique intended for photosensor applications. *Mater Res Bull*, 2012; 47: 3440-3444.[DOI]

[4] Pandya SG. Preparation and Characterization of Cadmium Sulphide Nanocrystalline Thin film grown by chemical method. *Int J Recent Sci Res*, 2016; 7: 14887-14890.

[5] Nikam CP, Gosavi SR. Characterization of nanocrystalline CdS thin films deposited on FTO by CBD for photosensor applications. *Advances Appl Sci Res*, 2014; 5: 267-272.

[6] Soliya V, Tandel D, Patel C et al. Effect of annealing time on optical and electrical properties of CdS thin films. *AIP Conf Proc*, 2018; 1961: 030025.[DOI]

[7] Izgorodin A, Winther-Jensen O, Winther-Jensen B et al. CdS thin-film electrodeposition from a phosphonium ionic liquid. *Phy Chem Chem Phys*, 2009; 11: 8532-8537.[DOI]

[8] Okorie O, Buba ADA, Ramalan AM. Optical and dielectric properties of cadmium sulphide thin film grown using chemical bath deposition technique. *IOSR J Appl Phys*, 2017; 9: 82-89.

[9] Khimani AJ, Chaki SH, Malek TJ et al. Cadmium sulphide (CdS) thin films deposited by chemical bath deposition (CBD) and dip coating techniques-a comparative study. *Mater Res Express*, 2018; 5: 036406.[DOI]

[10] Rafea MA, Farag AAM, Roushdy N. Controlling the crystallite size and influence of the film thickness on the optical and electrical characteristics of nanocrystalline Cu_2S films. *Mater Res Bull*, 2012; 47: 257-266.[DOI]

[11] Al-Taay HF. Preparation and Characterization of Chemical Bath Deposition synthesis CdS Nanocrystalline Thin Films. *Iraqi J Sci*, 2017; 58: 454-461.

[12] Bangal M, Ashtaputre S, Marathe S et al. Semiconducting Nanoparticles. *Hyperfine Interact*, 2005; 160: 81-94.[DOI]

[13] Shahzad MH, Awan AU, Akhtar S et al. Entropy and stability analysis on blood flow with nanoparticles through a stenosed artery having permeable walls. *Science Progress*, 2022; 105: 00368504221096000.[DOI]

[14] Saleem A, Akhtar S, Nadeem S. Bio-mathematical analysis of electro-Osmotically modulated hemodynamic blood flow inside a symmetric and nonsymmetric stenosed artery with joule heating. *Int J Biomath*, 2022; 15: 2150071.[DOI]

[15] Ghazwani HA, Akhtar S, Almutairi S et al. Insightful facts on peristalsis flow of water conveying multi-walled carbon nanoparticles through elliptical ducts with ciliated walls. *Front Phys*, 2022; 10: 551.[DOI]

[16] Akhtar S, McCash LB, Nadeem S et al. Convective heat transfer for Peristaltic flow of SWCNT inside a sinusoidal elliptic duct. *Sci Prog*, 2021; 104: 00368504211023683.[DOI]

[17] Koteswararao J, Satyanarayana SV, Madhu GM et al. Estimation of structural and mechanical properties of Cadmium Sulfide/PVA nanocomposite films. *Heliyon*, 2019; 5: e01851.[DOI]

[18] Darekar MS, Praveen BM. Synthesis and characterization of nanoparticles of semiconducting metal sulphide and their application. *Phys Scr*, 2022; 97: 065805.[DOI]

[19] Suresh S. Studies on the dielectric properties of CdS nanoparticles. Appl Nanosci, 2014; 4: 325-329.[DOI]

[20] Saraf R. High Efficiency and cost effective Cu_2S/CdS thin-film solar cell. *IOSR-JEEE*, 2012; 2: 47-51.

[21] Gurnani A, Inani H, Katharria YS et al. Synthesis of Cadmium Sulfide and Copper(I) Sulfide Nano-particles for Photovoltaic Devices. *Bionano Front*, 2015; 8: 144-145.

[22] Vogel W, Urban J, Kundu M et al. Sphalerite-Wurtzite intermediates in nanocrystalline CdS. *Langmuir*, 1997; 13: 827-832.[DOI]

[23] Mahdi MA, Kasem SJ, Hassen JJ et al. Structural and optical properties of chemical deposition CdS thin films. *Int J Nano Mater*, 2009; 2: 41-52.

[24] Chowdhury RI, Hossen MA, Mustafa G et al. Characterization of chemically deposited cadmium sulfide thin films. *Int J Mod Phys B*, 2010; 24: 5901-5911.[DOI]

[25] Uplane MD, Pawar SH. Effect of substrate temperature on transport and optical properties of sprayed Cd1-xZnxS films. *Solid State Commun*, 1983; 46: 847-850.[DOI]

[26] Dharmadasa IM, Bingham PA, Echendu OK et al. Fabrication of CdS/CdTe-based thin film solar cells using an electrochemical technique. *Coatings*, 2014; 4: 380-415.[DOI]